THE JOURNAL OF PHYSICAL CHEMISTRY A

Article

pubs.acs.org/JPCA

Dynamics Simulations and Statistical Modeling of Thermal Decomposition of 1-Ethyl-3-methylimidazolium Dicyanamide and 1-Ethyl-2,3-dimethylimidazolium Dicyanamide

Jianbo Liu,* Steven D. Chambreau,† and Ghanshyam L. Vaghjiani‡

Department of Chemistry and Biochemistry, Queens College and the Graduate Center of the City University of New York, 65-30 Kissena Boulevard, Queens, New York 11367, United States

†ERC, Inc., and ‡Propellants Branch, Aerospace Systems Directorate, Air Force Research Laboratory, AFRL/RQRP, Edwards Air Force Base, California 93524, United States

ABSTRACT: Quasi-classical, direct dynamics trajectories were calculated at the B3LYP/6-31G* level of theory, in an attempt to understand decomposition mechanisms of 1-ethyl-3-methylimidazolium dicyanamide ($EMIM^+DCA^-$) and 1-ethyl-2,3-dimethylimidazolium dicyanamide ($EMMIM^+DCA^-$). The trajectories showed many dissociation paths for these two ionic liquids. Using trajectory results as a guide, structures of transition states and products that might be important for decomposition of these two compounds were determined using density functional theory calculations. Rice–Ramsperger–Kassel–Marcus (RRKM) theory was then utilized to examine properties of energized ionic liquids and to determine unimolecular rates for crossing various transition states. On the basis of RRKM modeling, initial decomposition paths for energized $EMIM^+DCA^-$ correspond to formation of an *N*-heterocyclic carbene and acid pair via transfer of the C2 proton of $EMIM^+$ to DCA^-, and evolution of methylimidazole and ethylimidazole via S_N2 alkyl abstraction by DCA^-. Similar decomposition paths were identified for energized $EMMIM^+DCA^-$, except that the reactivity of C2 of the imidazolium cation is significantly reduced upon substitution of a methyl group for a hydrogen atom at this position. The present work demonstrates that dynamics simulations, in conjunction with statistical modeling, are able to provide insight into decomposition mechanisms, kinetics, and dynamics for alkylimidazolium-based ionic liquids and to predict product branching ratios and how they vary with decomposition temperatures.

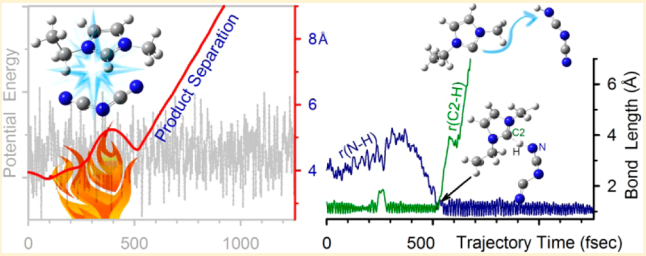

I. INTRODUCTION

The C2 proton of imidazolium cations is known to have acidic character, due to the stability of Arduengo-type[1] *N*-heterocyclic carbenes formed upon deprotonation of C2.[2] The acidity of the C2 site can lead to advantageous applications such as transition metal catalyzed reactions; however, it yields undesired and detrimental side reactions when using imidazolium-based ionic liquids as solvents.[3] This position could be rendered less acidic by replacing the hydrogen atom of C2 with a methyl group (even this methyl group is not completely inert and subject to deprotonation under mild conditions).[3] The facile deprotonation of the C2 position also affects the thermal stability of imidazolium-based ionic liquids during storage and transportation, and it appears that the thermal stability is enhanced for 2-substituted imidazolium ionic liquids.[4]

Imidazolium-based ionic liquids, when paired with dicyanamide anions, are expected to have solvating properties for a range of metal ions and carbohydrates[5] and may show a promising potential for propellant applications.[6,7] Thermal decomposition of 1-ethyl-3-methylimidazolium dicyanamide (i.e., $EMIM^+DCA^-$, $C_8H_{11}N_5$, molecular weight = 177.21) and 1-ethyl-2,3-dimethylimidazolium dicyanamide (i.e., $EMMIM^+DCA^-$, $C_9H_{13}N_5$, molecular weight = 191.23) has been investigated using thermogravimetric analysis (TGA) and isothermal TGA–mass spectrometry (TGA–MS) by the Air Force Research Laboratory (see companion article[8]). Thermal decomposition of $EMIM^+DCA^-$ initiates at ~590 K, and decomposition products (detected using an electron ionization source) include ethylimidazole (m/z 96) and methylimidazole (m/z 82). For comparison, thermal decomposition of $EMMIM^+DCA^-$ begins at ~640 K, and decomposition products include 1-ethyl-2-methylimidazole (m/z 110) and 1,2-dimethylimidazole (m/z 96). Both ionic liquids illustrate the importance of alkyl abstraction during pyrolysis, and the relative intensities of products change significantly with increasing the decomposition temperature.

The present work is to explore the thermal decomposition mechanisms of gaseous $EMIM^+DCA^-$ and $EMMIM^+DCA^-$ theoretically in an attempt to rationalize the differences observed in pyrolysis of these two ionic liquids and their correlations to the C2 activity of imidazolium cations. For complex molecules, especially for ionic liquids with high internal energy content, use of chemical intuition to predict

Received: September 22, 2014
Published: October 2, 2014

dx.doi.org/10.1021/jp5095849 | J. Phys. Chem. A 2014, 118, 11133–11144

reaction pathways can prove unreliable. There may exist concerted mechanisms and multiple competing initiation reactions that are difficult to predict.[9] Once the energy stored in the molecule begins to release, the system does not necessarily follow the minimum energy reaction path, i.e., the subsequent behavior is controlled by dynamics,[10] and the reaction may be autocatalytic.[4] Even for the reactions that are controlled by statistical factors, standard transition state locating methods may be difficult to apply because molecular transformations are too complex. A useful approach to treating such systems is quasi-classical, direct dynamics trajectory simulations, where the motion of the molecule is followed allowing the molecule to show us what the preferred reaction pathways are. One beneficial aspect of the direct dynamics method is that it dispenses with the potential energy surface. Instead, it calculates the energies, force constants, and Hessian "on the fly" using quantum chemistry methods.[11−19] This method becomes computationally attractive when the dimensionality of the system increases. Dynamics simulations partition the heat provided to the system and the energy generated by the reactions into vibrational, rotational, and translational modes, increasing the chance of locating new reaction pathways. In addition, by following the variation of the potential energy during trajectories rather than relying on intuition, we can identify better geometries for TS searching. As exemplified by our recent study on thermal decomposition of 1,5-dinitrobiuret (DNB),[9] direct dynamics trajectory simulations act as a powerful guide for investigating decomposition mechanisms and dynamics of complex energetic molecules.

In the present work, quasi-classical, direct dynamics trajectory simulations were performed for decomposition of $EMIM^+DCA^-$ and $EMMIM^+DCA^-$, respectively. Using trajectory results as a guide, reaction coordinates for their decomposition were mapped out using density functional theory (DFT) electronic structure calculations. Rice−Ramsperger−Kassel−Marcus (RRKM) theory[20] was then employed to examine statistical dissociation behaviors of these two ionic liquids at elevated temperatures. Dynamics simulations, in conjunction with statistical modeling, helped us extract mechanisms, kinetics, dynamics, and product branching ratios for the thermal decomposition of these two imidazolium-based ionic liquids. The reminder of the article is organized as follows. In section II, methodologies of DFT calculations, RRKM modeling, and quasi-classical direct dynamics simulations are described. Trajectory simulation results are presented in section III, including an overview of the nature and time scales of trajectories, sorting of decomposition paths, and contributions of various decomposition paths to $EMIM^+DCA^-$ and $EMMIM^+DCA^-$. Statistical modeling results are presented in section IV, starting with construction of the reaction coordinates for decomposition of $EMIM^+DCA^-$ and $EMMIM^+DCA^-$ using DFT calculations, proceeding to RRKM decomposition rates and product branching, and their dependence on temperature. Conclusions are presented in section V.

II. COMPUTATIONAL METHODOLOGIES

A. Electronic Structure and RRKM Calculations. To aid in reaction coordinate interpretation, DFT calculations were performed at the B3LYP/6-31+G* level of theory, using the Gaussian 09 (B.01) suite of programs.[21] The B3LYP method applied to many dialkylimidazolium-based ionic liquids with reasonable results[22−25] and resulted in negligible basis set superposition error (BSSE) in dissociation energy calculations.[24] One concern is that B3LYP may not adequately represent potential energy surfaces of ionic liquids making them deeper than they should be, and B3LYP may particularly favor the ion pair interaction in which the anion interacts with the C2−H. We have compared the ion-pairing energies of $EMIM^+DCA^-$ and $EMMIM^+DCA^-$ at B3LYP/6-31+G(d) and M062-X/6-31+G(d). It was found that B3LYP/6-31+G(d) calculated potentials are actually 7−8% less than those by M062-X/6-31+G(d). The two methods yielded identical energetics for the proton transfer between separated $EMIM^+$ and DCA^- and between $EMMIM^+$ and DCA^-. Unfortunately M062-X/6-31+G(d) occasionally ran into convergence failure. Note that our aim is to predict the decomposition behaviors of $EMIM^+DCA^-$ and $EMMIM^+DCA^-$ rather than provide the most accurate structures, and B3LYP has proven to be a useful tool to predict thermal decomposition mechanisms and temperatures of dialkylimidazolium-based ionic liquids.[26]

Geometries were optimized by calculating force constants at every step. All of the transition states (TSs) found were verified to be first-order saddle points by frequency calculations, and the vibrational mode with an imaginary frequency corresponds to the associated reaction pathway. Vibrational frequencies and zero-point energies (ZPE) were scaled by a factor of 0.955 and 0.981,[27] respectively. The corrected ZPE were added to the stationary-point energies. The molecular structures of reactants, TSs, and products are available by request from the corresponding author.

A transition-state-theory-based statistical model, RRKM theory,[20] was employed to examine the properties of energized reactants and transition states as a function of total internal energy and associated angular momentum. The fundamental assumption in the RRKM model is that energy is randomized and distributed statistically among all the energetically accessible states of the system, and the rate of a particular process (e.g., dissociation of a molecule) is proportional to the total number of energetically accessible states at the transition state.[28,29] As a consequence, statistical reactions tend to occur by paths close to the minimum energy route, as the density of states is highest for such paths.[30] Therefore, an accurate description of the reaction coordinate is a prerequisite to statistical modeling. RRKM densities of states and unimolecular rates for crossing various transition states were calculated with the program of Zhu and Hase,[31] using its direct count algorithm, and scaled frequencies and energetics from DFT calculations. The angular momentum quantum number J used for RRKM calculations was determined from the corresponding reactant rotational energy, assuming both $EMIM^+DCA^-$ and $EMMIM^+DCA^-$ can be roughly treated as nearly symmetric top molecules since each molecule has two principle moments of inertia, which are not very different. Product branching is given by the ratio of the RRKM rates.

B. Quasi-Classical Direct Dynamics Trajectory Simulations. In this work, direct dynamics trajectory simulations were conducted for two purposes: (1) probing gross decomposition features of two ionic liquids, discovering decomposition products, and investigating different decomposition mechanisms of $EMIM^+DCA^-$ vs $EMMIM^+DCA^-$; and (2) locating key transition states for important decomposition paths, when standard TS-searching methods (i.e., TS, QST2, and QST3 methods in Gaussian) fail.[9,32,33] Trajectory simulations started at the equilibrium geometries of $EMIM^+DCA^-$ and $EMMIM^+DCA^-$, respectively. A chemical

dx.doi.org/10.1021/jp5095849 | J. Phys. Chem. A 2014, 118, 11133−11144

dynamics program VENUS of Hase et al.[34] was used to set up trajectory initial conditions. The Hessian-based predictor-corrector algorithm of Schlegel and co-workers,[19] implemented in Gaussian, was used for numerical integration of the classical equations of motion, with the Hessian matrix updated every five steps. The integrations were performed with a step size of ~0.3 fs, which was small enough for SCF convergence as well as to keep the total energy constant. The initial guess of molecular orbital for each DFT calculation was obtained from the previous trajectory step, and the total energy of the system was checked during the simulation to ensure the energy was conserved to better than 10^{-4} Hartree. The SCF = XQC option was adopted for the trajectory integration so that a quadratically convergent SCF method[21,35] was used in case the usual but much faster, first-order SCF method failed to converge within the allotted number of cycles. Because millions of gradient and Hessian evaluations were required, the level of theory used for simulations was necessarily modest. On the basis of computational speed and the overall level of agreement with high level results, B3LYP/6-31G* was chosen as the level of theory for calculating trajectories.

Initial quantum numbers of the reactant vibrational modes were sampled using the quantum Boltzmann probability distribution

$$P(n_i) = \exp\left(-\frac{n_i h\nu_i}{k_B T}\right)\left[1 - \exp\left(-\frac{h\nu_i}{k_B T}\right)\right] \quad (1)$$

where ν_i and n_i are the vibrational frequency and quantum number of the ith mode, respectively, and T is the simulation temperature. Rotational energy was added by sampling the classical Boltzmann distribution.[36] Quasi-classical vibrational states were simulated by giving individual reactant atoms displacements from equilibrium and momenta that are appropriate to the initial rovibrational state, with random phases for different modes. Each molecule has ZPE in all vibrational modes. Because the decomposition time scale at typical pyrolysis temperatures would be far too long for practical trajectories, simulations have to be carried out at a high temperature. To identify a reasonable temperature for dynamics simulations, we first ran a series of trajectories for $EMIM^+DCA^-$ using a low level of theory HF/3-21G, in a temperature range from 1000 to 8000 K with an interval of 1000 K. Each trajectory was propagated for a period of ~5.1 ps. Only 20%, 46%, and 45% of trajectories are dissociative at 1000, 2000, and 3000 K, respectively. All these reactive trajectories formed *N*-heterocyclic carbenes only. At temperature above 4000 K, almost every trajectory formed *N*-heterocyclic carbene or underwent dealkylation, followed by secondary decompositions within a short time (<2 ps). Therefore, 4000 K was chosen for running trajectory simulations for both $EMIM^+DCA^-$ and $EMMIM^+DCA^-$ at the B3LYP/6-31G* level of theory. For each compound, batches of trajectories (63 trajectories for $EMIM^+DCA^-$ and 85 for $EMMIM^+DCA^-$) were calculated. Trajectories were terminated after a preset length of time (~3 ps), or when the product separation exceeded 9.0 Å. A total of 148 trajectories were completed at the B3LYP/6-31G* level of theory in the course of the work reported here. On average, each trajectory took ~760 CPU hours on an Intel core i7 6-core (3.2 GHz)-based 64 bit Linux workstation cluster, and the complete set of trajectories were obtained at a cost of 13 years of CPU time on the cluster. The program gOpenMol was used for trajectory visualization.[37] Analysis of individual trajectories and statistical analysis of the trajectory ensemble was done with programs written for this purpose.[9,33,38−43]

One issue with using quasi-classical trajectory methods is that vibrational energy is not quantized in molecules. Lack of quantization presumably has an effect on how energy is distributed between vibrational modes during trajectories and upon dissociation.[44,45] It is possible to have trajectories where the product vibrational energy is below the zero-point level. Such unphysical trajectories were found to be negligible in our trajectories, presumably because we are looking at high internal energies (see Table 1), reducing the errors associated with treating the motion classically.

Table 1. Calculated Vibrational and Rotational Energies of Reactants at Various Temperatures

temperature (K)	298	750	1000	1250	4000
E_{vib} of $EMIM^+DCA^-$ (eV)	0.33	1.66	2.67	3.78	18.34
E_{vib} of $EMMIM^+DCA^-$ (eV)	0.37	1.88	3.02	4.28	20.80
E_{rot} (eV)	0.04	0.1	0.13	0.16	0.52

As mentioned above, the temperature used for the simulations is much higher than the decomposition temperature in a typical pyrolysis source, e.g. , 500−650 K in TGA experiments.[8] Table 1 lists the estimated vibrational and rotational energies for $EMIM^+DCA^-$ and $EMMIM^+DCA^-$ at various temperatures. As a result, some trajectories may find decomposition paths with barriers too high to be relevant to decomposition at realistic temperatures. The trajectory observables of greatest interest for our purpose are decomposition mechanisms. The point is that with enough trajectories, *all* important reaction paths will be found, including those that control decomposition under the conditions of interest. Once decomposition paths are identified, the corresponding reaction energetics including activation barriers can be calculated, and only those that are able to contribute need to be included in decomposition kinetics modeling.

III. TRAJECTORY RESULTS

A. $EMIM^+DCA^-$. Before discussing the trajectory results for $EMIM^+DCA^-$, it is useful to review the nature and time scales of these trajectories. Trajectories were run at 4000 K. At this temperature, 7% of trajectories maintained an intact ion pair structure when trajectories were terminated at 3 ps. The remaining 93% of trajectories underwent thermal decomposition via direct and sequential mechanisms. For most of the decomposition trajectories, the time at which the molecule begins decomposition is between 0.2 and 1 ps, longer than the periods of most vibrational modes of $EMIM^+DCA^-$. The decomposition trajectories can be grouped into six classes, as described below along with their contributions (i.e., trajectory ratios). The structures of $EMIM^+DCA^-$ and its decomposition products observed in trajectories are depicted in Figure 1. All these structures were optimized at the B3LYP/6-31+G* level of theory. Note that both $EMIM^+DCA^-$ and $EMMIM^+DCA^-$ ion pairs were fully conformationally screened at the B3LYP/6-31+G* level to ensure that their global minima (rather than local minima) were used as starting geometries for trajectories. During structure optimizations of the ion pairs, individual ions in their lowest energy conformations were used as starting points,[5,46] and all conformations arising from the rotation of

dx.doi.org/10.1021/jp5095849 | J. Phys. Chem. A 2014, 118, 11133−11144

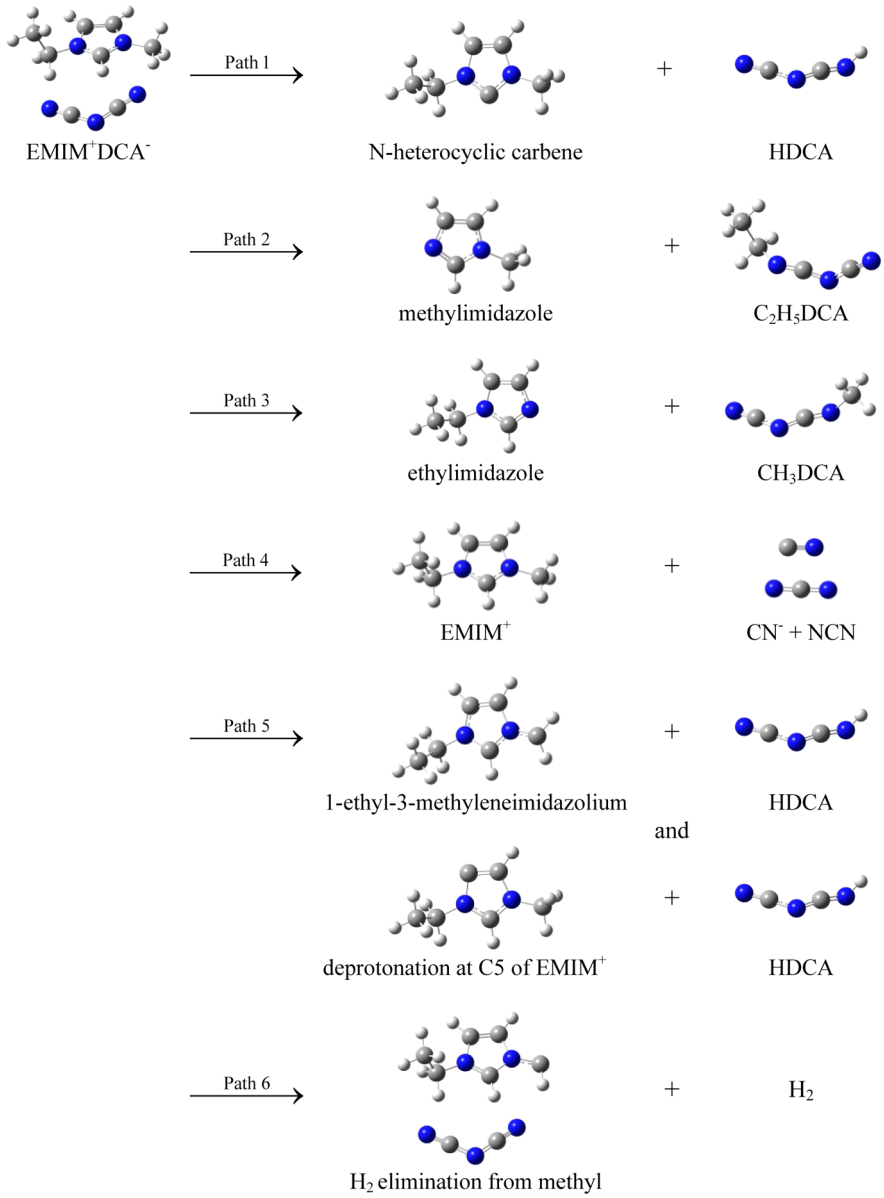

Figure 1. B3LYP/6-31+G* optimized structures of $EMIM^+DCA^-$ and its decomposition products.

DCA^- vs imidazolium ring were explored. In the DFT-calculated lowest energy conformation of $EMIM^+DCA^-$, DCA^- interacts with $EMIM^+$ from the C2 side and is roughly in parallel with the plane of the imidazolium ring. It is important to note that, at the simulation temperature of 4000 K, the reactant was vigorously excited due to high internal energy. Consequently, although a global minimum conformation was set as the starting $EMIM^+DCA^-$ conformation for trajectories, the reactant actually existed as a mix of various conformations in trajectories. In other words, all energetically accessible conformations of $EMIM^+DCA^-$ (or $EMMIM^+DCA^-$) were involved in trajectory simulations of thermal decomposition. This represents the nature of direct dynamics simulations, which is to follow the motion of molecules and let trajectories show what the preferred conformer(s) and decomposition pathways are.

Decomposition Path **1** *(Formation of N-Heterocyclic Carbene).* One common outcome of $EMIM^+DCA^-$ decomposition is path **1**, where an *N*-heterocyclic carbene product (i.e., 1-ethyl-3-methyl-imidazole-2-ylidene, EMIM:) is formed via proton transfer from C2 of $EMIM^+$ to a terminal N atom of DCA^-. This path accounts for 31% of all trajectories. The reaction enthalpy is 1.29 eV. Figure 2 demonstrates a trajectory representative of path **1**. The top frame of the figure shows the change in potential energy (PE) and CM distance along the trajectory time, and the bottom frame shows the r(C2−H) and r(N−H) bond lengths breaking or forming during proton transfer. The CM distance is the distance between the centers of mass of the reactant ion pair or decomposition products. The oscillation in the PE reflects the vibration of $EMIM^+DCA^-$ and products, including ZPE. It is obvious that the time scale of decomposition depends on the simulation temperature. In this trajectory, proton transfer between $EMIM^+$ and DCA^- occurs around 520 fs. After proton transfer, some trajectories of path **1** experienced subsequent decomposition of the *N*-heterocyclic carbene.

Decomposition Path **2** *(Elimination of Ethyl).* Another major mode of $EMIM^+DCA^-$ decomposition belongs to path **2**,

dx.doi.org/10.1021/jp5095849 | J. Phys. Chem. A 2014, 118, 11133−11144

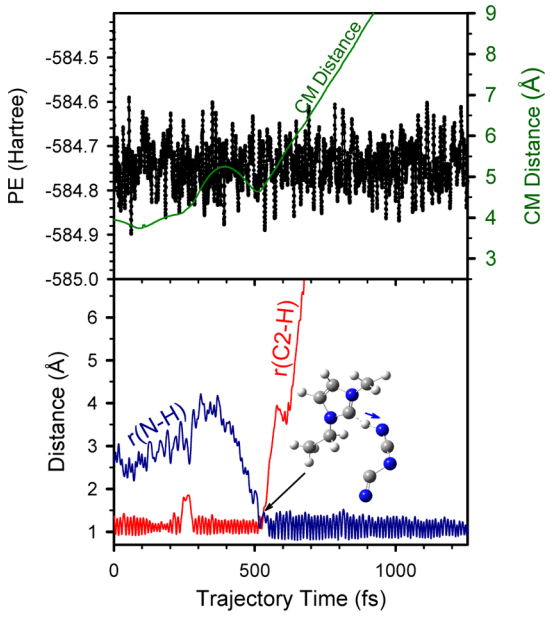

Figure 2. Representative trajectory of decomposition path **1** for $EMIM^+DCA^-$, simulated at 4000 K. (top) The variation in the potential energy and the CM distance between the reactant ion pair or the product carbene acid pair, and (bottom) the variation in various bond lengths during the trajectory. Snapshot shows proton transfer from the C2 position of $EMIM^+$ to DCA^-, as indicated by the blue arrow.

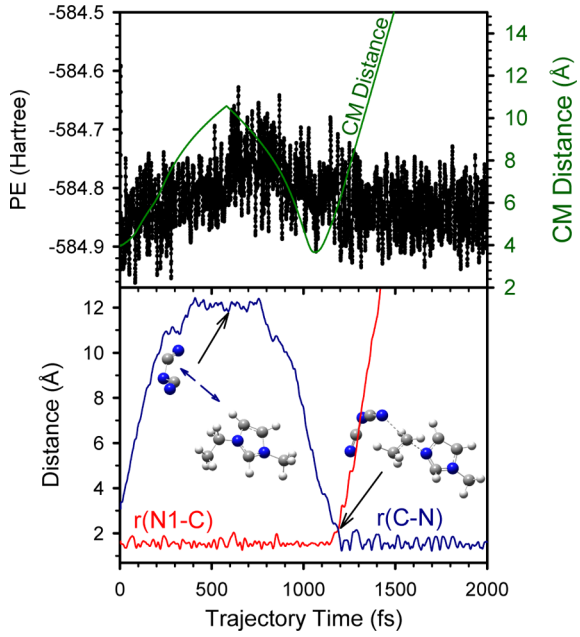

Figure 3. Representative trajectory of decomposition path **2** for $EMIM^+DCA^-$, simulated at 4000 K. (top) The variation in the potential energy and the CM distance between the $EMIM^+$ and DCA^- ion pair in the reactant or methylimidazole and C_2H_5DCA in the products, and (bottom) the variation in various bond lengths during the trajectory. Two snapshots show the separation of the ion pair and S_N2 ethyl abstraction, respectively.

accounting for nearly 30% of all trajectories. Of these trajectories, most went through direct elimination of the ethyl group from the N1 position; only a few underwent ethyl abstraction via an S_N2 type mechanism, yielding methylimidazole and C_2H_5DCA. However, according to the reaction coordinate and RRKM modeling (*vide infra*), the S_N2 mechanism is endothermic by only 0.10 eV and involves a much lower energy barrier than the direct elimination mechanism, and thus accounts for most of the ethyl elimination from $EMIM^+DCA^-$ under typical pyrolysis conditions. A trajectory representative of S_N2 ethyl abstraction is illustrated in Figure 3, showing the changes in PE and CM distance in the top frame, and the breaking of r(N1−C) in $EMIM^+$ and the forming of new r(C−N) in C_2H_5DCA in the bottom frame. The plot of PE indicates two activated decomposition steps. The first energy barrier represents dissociation of the $EMIM^+DCA^-$ ion pair into two individual ions separated by 10.6 Å at 580 fs as shown in the snapshot inserted to the left, while the second one represents the S_N2 ethyl abstraction from $EMIM^+$ by DCA^- at 1190 fs as shown in the snapshot inserted to the right, followed by the separation of neutral products methylimidazole and C_2H_5DCA. During ethyl abstraction, the molecule has a linear N1−C−N geometry with a nearly planar $-CH_2CH_3$ group, which resembles a transition state for typical S_N2-type dealkylation of imidazolium-based ionic liquids.[47]

Decomposition Path ***3*** *(Elimination of Methyl).* Elimination of methyl contributes to 10% of all $EMIM^+DCA^-$ trajectories at 4000 K, referred to as path **3**. Analogous to the trajectories of path **2**, some trajectories of path **3** experienced direct elimination of the methyl group from the N3 position, while others underwent methyl abstraction via an S_N2 mechanism, yielding ethylimidazole and CH_3DCA with a reaction enthalpy of 0.12 eV. Similar to ethyl elimination of $EMIM^+DCA^-$, at typical ionic liquid decomposition temperatures direct methyl elimination route is less likely to contribute to a significant extent. The S_N2 route accounts for most of the methyl elimination. Figure 4 shows a typical S_N2 methyl elimination. In this trajectory, the $EMIM^+DCA^-$ ion pair first

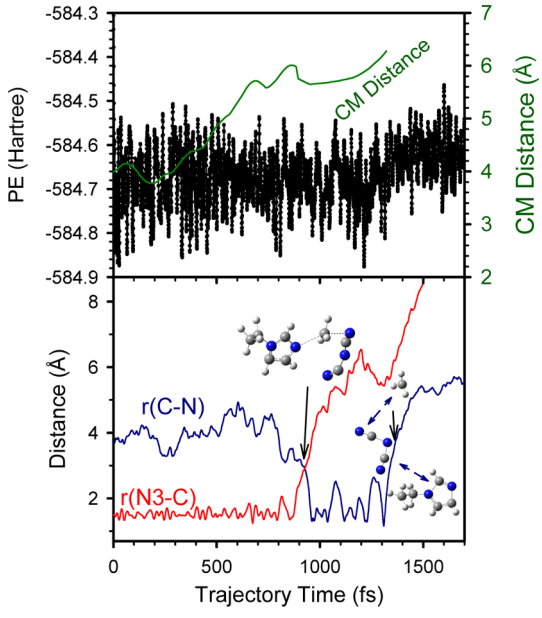

Figure 4. Representative trajectory of decomposition path **3** for $EMIM^+DCA^-$, simulated at 4000 K. (top) The variation in the potential energy and the CM distance between the $EMIM^+$ and DCA^- ion pair in the reactant or ethylimidazole and CH_3DCA in the products, and (bottom) the variation in various bond lengths during the trajectory. Two snapshots show S_N2 methyl abstraction and fragmentation of primary product CH_3DCA, respectively.

dx.doi.org/10.1021/jp5095849 | J. Phys. Chem. A 2014, 118, 11133−11144

Table 2. Trajectory Simulation Results for the Decomposition of EMMIM$^+$DCA$^-$ at 4000 K

Path	Decomposition products	ΔH^a (eV)	Ratio^b (%)
1	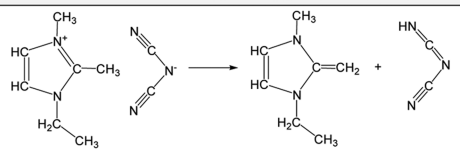	1.41	18 ± 4
2	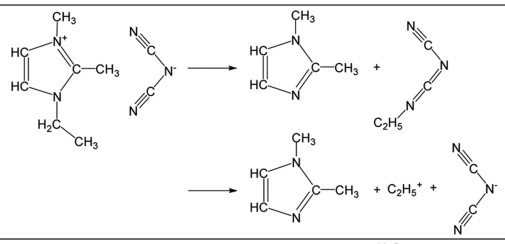	0.16 -	34 ± 5
3	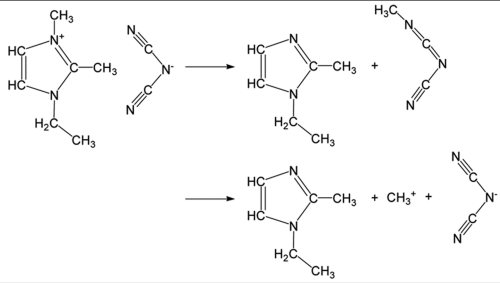	0.19 -	11 ± 3
4	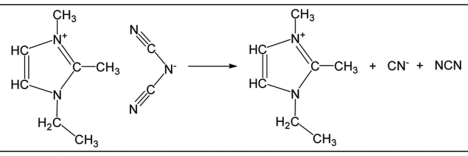	8.62	9 ± 3
5	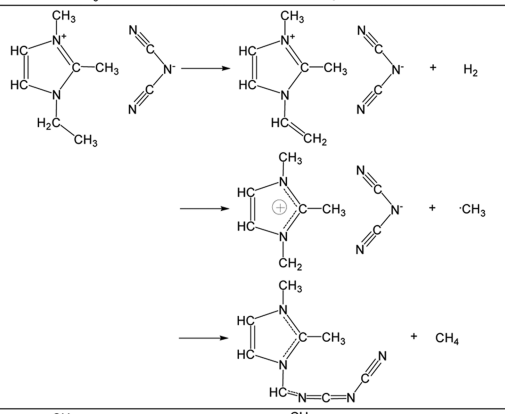	1.37 3.48 1.78	12 ± 3
6	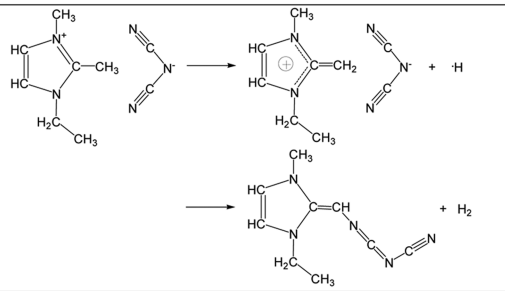	3.80 1.64	8 ± 3
7	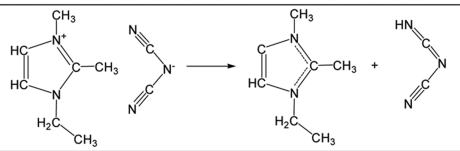	2.19	3 ± 2
	Non-reactive	0	5 ± 2

^{a}Values of ΔH were calculated relative to EMIM$^+$DCA$^-$, at the B3LYP/6-31+G* level of theory. ^{b}Trajectory ratios were calculated based on 85 trajectories.

dx.doi.org/10.1021/jp5095849 | J. Phys. Chem. A 2014, 118, 11133−11144

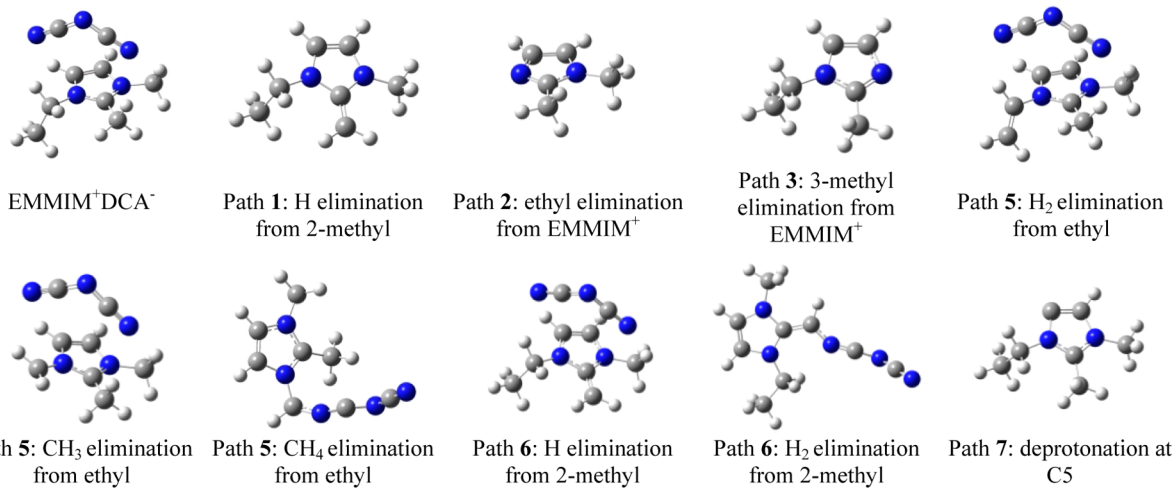

Figure 5. B3LYP/6-31+G* optimized structures of $EMMIM^+DCA^-$ and its decomposition products.

separates to a CM distance of ~6.0 Å, then the DCA^- anion abstracts the methyl group from the N3 of $EMIM^+$ via an intramolecular S_N2 mechanism to form ethylimidazole and CH_3DCA (at 927 fs, the left snapshot). In Figure 4, CH_3DCA further decomposes to CH_3 and DCA (starts at 1350 fs, the right snapshot). Note that methyl group may also be abstracted by the central N atom of DCA^-, producing neutral product $NCN(CH_3)CN$. However, previous DFT calculations indicate that the barrier to form the terminally methylated dicyanamide should be lower than for the centrally methylated product.[48] Also, in the temperature jump FTIR measurement of a similar ionic liquid 1-butyl-3-methylimidazolium dicyanamide ($BMIM^+DCA^-$), methylation of the terminal nitrogen on DCA better matches the experimental spectra.[8]

Other Decomposition Paths. Remaining trajectories can be characterized as paths **4**, **5**, and **6**, accounting for 10%, 8%, and 4% of all $EMIM^+DCA^-$ trajectories, respectively. Path **4** involves decomposition of the DCA^- anion only, producing CN^- and neutral NCN, which is endothermic by 8.68 eV (i.e., the sum of the ion pair binding energy and DCA^- dissociation energy). In some path **4** trajectories, proton transfer occurs between C2 of $EMIM^+$ and CN^-, generating an *N*-heterocyclic carbene and HCN (or HNC). Path **5** corresponds to the transfer of a proton to the DCA^- anion either from 3-methyl or from C5 of the imidazolium ring, with reaction endothermicity of 2.48 and 2.07 eV, respectively. Finally, H_2 elimination from 3-methyl of the imidazolium ring was observed in path **6** with a reaction enthalpy of 4.03 eV, but this path is much less common.

B. $EMMIM^+DCA^-$. The decomposition trajectories of $EMMIM^+DCA^-$ can be grouped into seven classes, as summarized in Table 2. Structures of the lowest energy conformation of $EMMIM^+DCA^-$ and its decomposition products are depicted in Figure 5, except those of CN^-, NCN, HDCA, CH_3DCA, and C_2H_5DCA, which are included in Figure 1. Note that the global minimal conformation of $EMMIM^+DCA^-$ is found to have the anion interacting with the cation from the top of the imidazolium ring, which is different than the side conformation for the global minimum of $EMIM^+DCA^-$ shown in Figure 1. Table 2 also compares their product energetics and relative contributions. The error limits given for the trajectory ratios are statistical, based on the number of total trajectories and reactive trajectories for each path, and obviously do not include any systematic errors.

Major decomposition paths of $EMMIM^+DCA^-$ include proton transfer from the 2-methyl group of $EMMIM^+$ to DCA^-, elimination of the ethyl and 3-methyl groups from $EMMIM^+$, and dissociation of the DCA^- anion. Figure 6 shows

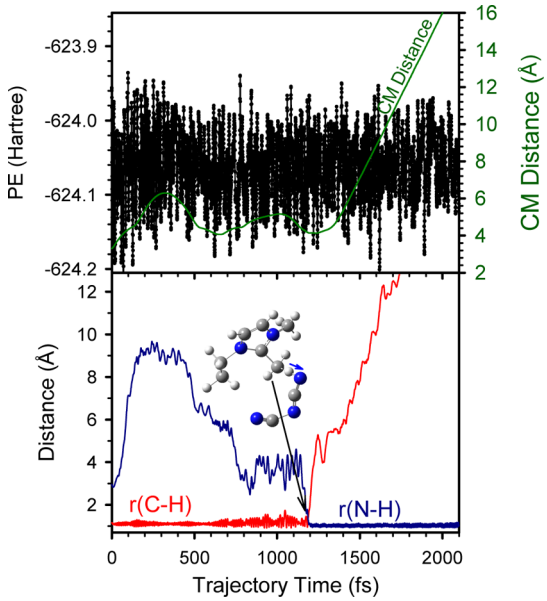

Figure 6. Representative trajectory of decomposition path **1** for $EMMIM^+DCA^-$, simulated at 4000 K. (top) The variation in the potential energy and the CM distance between the reactant ion pair or decomposition products, and (bottom) the variation in various bond lengths during the trajectory. Snapshot shows proton transfer from 2-methyl of $EMMIM^+$ to DCA^-, as indicated by the blue arrow.

a typical proton transfer reaction between $EMMIM^+$ and DCA^-, for comparison with the proton transfer between $EMIM^+$ and DCA^- (Figure 2). Similar to that seen in $EMIM^+DCA^-$, most methyl- and ethyl-elimination trajectories of $EMMIM^+DCA^-$ occur directly due to the high simulation temperature; only a few are mediated by S_N2 mechanisms and yield CH_3DCA and C_2H_5DCA, respectively. We also observed H_2, CH_3, and CH_4 elimination from 1-ethyl, and H and H_2 elimination from 2-methyl of $EMMIM^+$.

dx.doi.org/10.1021/jp5095849 | J. Phys. Chem. A 2014, 118, 11133−11144

C. Trajectory Validation. Before analyzing the decomposition mechanisms of $EMIM^+DCA^-$ and $EMMIM^+DCA^-$ based on trajectory results, it is important to verify that the trajectories are in reasonable agreement with general decomposition behaviors of imidazolium-based ion liquids as well as recent AFRL experimental results of these two ionic liquids. The trajectories reveal many similarities between major decomposition pathways of these two ionic liquids and lead us to predict that paths **1**, **2**, and **3** may represent typical decomposition paths of $EMIM^+DCA^-$ and $EMMIM^+DCA^-$, particularly in view of their initial decomposition steps.

These paths are chosen for several considerations. First, all three paths are energetically more favorable and attained much higher probabilities than others in trajectory simulations. Second, formation of carbene−acid pair has been identified in thermal decomposition of 1,3-dialkylimidazolium-based ionic liquids, such as $EMIM^+$acetate$^-$ [2,49] and $EMIM^+Cl^-$.[50] S_N2 alkyl abstraction has also been reported for many imidazolium-based ionic liquids,[4,47] such as $EMIM^+$acetate$^-$, $EMMIM^+$acetate$^-$,[49] $EMIM^+Br^-$,[47] and other EMIM halide ionic liquids.[51] Particularly, the products identified in paths **1**, **2**, and **3** were observed in recent TGA−MS and vacuum ultraviolet photoionization time-of-flight mass spectrometry (VUV−PI−TOFMS) measurements of corresponding ionic liquids, including *N*-heterocyclic carbene (i.e., loss of 1 amu from $EMIM^+$, m/z 110), methylimidazole, and ethylimidazole for $EMIM^+DCA^-$, and 1-ethyl-2-methylene-3-methylimidazolium (i.e., loss of 1 amu from $EMMIM^+$, m/z 124), 1-ethyl-2-methyl imidazole, and 1,2-dimethyl imidazole for $EMMIM^+DCA^-$, respectively.[8] Note that no CH_3DCA or C_2H_5DCA were observed in the MS measurements. This is because polymerization prohibits the vaporization of these species. Finally, the major difference between thermal decomposition trajectories of $EMIM^+DCA^-$ and $EMMIM^+DCA^-$ is observed in the proton transfer reactions between ion pairs. For $EMIM^+DCA^-$, proton transfer originates from C2 of the $EMIM^+$ ring and has the highest reaction probability in trajectories; whereas for $EMMIM^+DCA^-$ proton transfer originates from the 2-methyl group of $EMMIM^+$, and the reaction probability decreases in trajectories. This is consistent with the experimental observation, i.e., VUV−PI−TOFMS revealed a significant loss of 1 amu from $EMIM^+$, but loss of 1 amu from $EMMIM^+$ occurred to a lesser extent.[8]

Overall, our trajectory results are in good agreement with literature and experimental results. We therefore feel confident in using trajectories as a guide to extract additional mechanistic insight. Note that path **4**, dissociation of DCA^- anions, has a significant ratio in trajectories of both ionic liquids; however, the large decomposition endothermicity (i.e., 5.31 eV for $DCA^- \rightarrow CN^- + NCN$ in addition to the 3.3−3.4 eV ion pair binding energy) renders this route improbable at pyrolysis temperatures below 1250 K.

IV. RRKM MODELING

A. Reaction Coordinates. DFT-calculated reaction coordinates for the initial decomposition of $EMIM^+DCA^-$ and $EMMIM^+DCA^-$ are summarized in Figures 7 and 8, respectively, with the reactant molecules shown near the center at zero energy. All energetics were calculated at the B3LYP/6-31+G* level of theory. Structures of various TSs were obtained using likely high potential energy geometries in reactive trajectories as starting geometries for optimization.

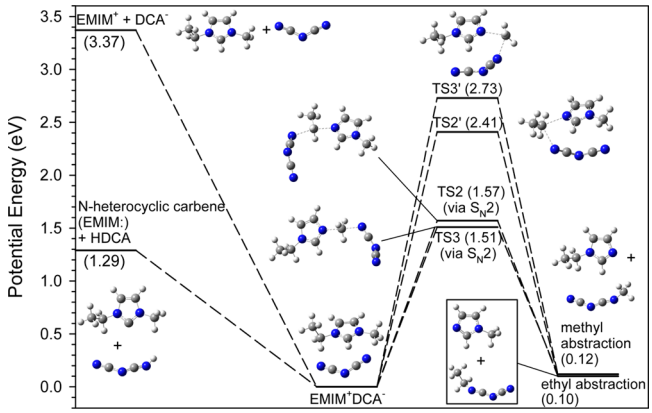

Figure 7. Schematic reaction coordinate for the initial decomposition of $EMIM^+DCA^-$. Energetics (eV) of TSs and products are derived from B3LYP/6-31+G* calculations, including ZPE.

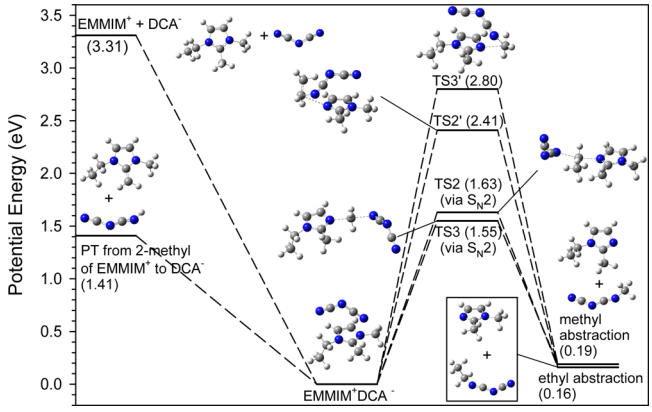

Figure 8. Schematic reaction coordinate for the initial decomposition of $EMMIM^+DCA^-$. Energetics (eV) of TSs and products are derived from B3LYP/6-31+G* calculations, including ZPE.

$EMIM^+DCA^-$. In Figure 7, proton transfer leading to *N*-heterocyclic carbene EMIM: and HDCA (i.e., path **1**) needs no complicated rearrangement. Efforts were made to locate a transition state connecting $EMIM^+DCA^-$ to the products EMIM: + HDCA. However, various starting geometries corresponding to a dissociating C−H bond at C2 of $EMIM^+$ converged, instead, to the $EMIM^+$ structure at B3LYP/6-31+G* level. Relaxed potential energy scans were performed along the proton transfer from C2 of $EMIM^+$ to one terminal N of DCA^-, or from product HDCA back to the C2 position of EMIM:. PES scans continuously varied the dissociating r(C2−H) bond length of $EMIM^+$ from 1.08 to 2.03 Å or the new r(N−H) of HDCA from 2.36 to 0.95 Å, and optimized all coordinates other than r(C2−H) or r(N−H) at each point. Both PES scans show no substantial energy barriers associated with proton transfer. It is therefore expected that formation of EMIM: opens at the thermodynamic threshold energy of 1.29 eV. This finding is similar to that for $EMIM^+Br^-$[47] in which proton transfer from HBr to EMIM: to form the $EMIM^+Br^-$ ion pair occurs without an energy barrier, and to those for 1-butyl-3-methylimidazolium tetrafluoroborate ($BMIM^+BF_4^-$) and 1-butyl-3-methylimidazolium hexafluorophosphate ($BMIM^+PF_6^-$)[48] in which the transfer of the proton on C2 of $BMIM^+$ to either of the two anions is an endothermic reaction resulting in formation of a BMIM: carbene, HF and BF_3 or PF_5, but does not have a transition state.

dx.doi.org/10.1021/jp5095849 | J. Phys. Chem. A 2014, 118, 11133−11144

Table 3. RRKM Results for the Initial Decomposition of $EMIM^+DCA^-$ and $EMMIM^+DCA^-$

	$EMIM^+DCA^-$			$EMMIM^+DCA^-$		
temperature (K)	750	1000	1250	750	1000	1250
	Unimolecular Rates (s^{-1})[a]					
k_1	1.13×10	3.65×10^5	3.48×10^7	3.15	2.12×10^5	2.92×10^7
k_2	2.39×10^{-4}	1.27×10^4	5.36×10^6	9.81×10^{-2}	4.12×10^5	1.60×10^8
k_3	1.76×10^{-2}	4.85×10^4	1.28×10^7	1.49×10^{-1}	5.84×10^4	1.30×10^7
Σk_i	1.13×10	4.26×10^5	5.30×10^7	3.39	6.92×10^5	2.02×10^8
	Branching Ratios (%)					
path **1** (proton transfer)	99.8	85.6	65.8	92.7	32.0	14.4
path **2** (ethyl abstraction)	0	3.0	10.1	2.9	59.6	79.1
path **3** (methyl abstraction)	0.2	11.4	24.1	4.4	8.4	6.5

[a] k_1, k_2, and k_3 are the rate constants for crossing TS1, TS2, and TS3 from the reactants, respectively.

A possible low energy route located computationally for path **2** (i.e., elimination of ethyl) appears to be $EMIM^+DCA^- \rightarrow$ TS2 $\rightarrow$ methylimidazole + C_2H_5DCA via an S_N2 abstraction mechanism. The reaction is endothermic by 0.10 eV; however, the decomposition path bears an energy barrier of 1.57 eV with respect to $EMIM^+DCA^-$. Path **3** (i.e., elimination of methyl) is analogous to path **2**, following $EMIM^+DCA^- \rightarrow$ TS3 $\rightarrow$ ethylimidazole + CH_3DCA, with the activation barrier at TS3 being 1.51 eV above $EMIM^+DCA^-$. The activation barrier for S_N2 ethyl abstraction is 0.06 eV higher than that for S_N2 methyl abstraction. This is similar to the observation on $EMIM^+Br^-$, in which the activation enthalpy for ethyl abstraction increases by 0.07 eV versus methyl abstraction due to steric factors.[47] One issue for interpretation of paths **2** and **3** products is that methyl and ethyl could be eliminated directly as illustrated in the trajectories, followed by the addition of the ethyl or methyl group to DCA. Figure 7 also shows the associated barriers at TS2′ (2.41 eV above the reactant) and TS3′ (2.73 eV above the reactant) for these two alternative routes. These calculated energy barriers are equivalent to the dissociation thresholds of C_2H_5 and CH_3 from $EMIM^+DCA^-$, respectively; therefore, in the latter mechanism, elimination of the alkyl group is the rate-limiting step followed by formation of alkyl DCA. No other low energy routes were found for decomposition paths **1**, **2**, and **3**, although we cannot exclude the possibility that such routes exist. We also include in the figure the binding energy of the $EMIM^+DCA^-$ ion pair, which is 3.37 eV calculated by dissociating the intact ion pair into two separated ions.

$EMMIM^+DCA^-$. $EMMIM^+DCA^-$ has a similar decomposition PES (see Figure 8) as that of $EMIM^+DCA^-$. As confirmed by relaxed PES scans running along the proton transfer from 2-methyl of $EMMIM^+$ to DCA^-, there is no reverse barrier associated with proton transfer of path **1**. $EMMIM^+DCA^-$ also follows S_N2 mechanisms as in the $EMIM^+DCA^-$ case, i.e., $EMMIM^+DCA^- \rightarrow$ TS2 (1.63 eV) $\rightarrow$ 1,2-dimethylimidazole + C_2H_5DCA (path **2**), and $EMMIM^+DCA^- \rightarrow$ TS3 (1.55 eV) $\rightarrow$ 1-ethyl-2-methylimidazole + CH_3DCA (path **3**). On the basis of the same argument for $EMIM^+DCA^-$, S_N2 methyl abstraction for $EMMIM^+DCA^-$ has a slightly lower activation barrier than that of ethyl abstraction, despite the fact that the reaction enthalpy for ethyl abstraction is less endothermic. We also calculated the energy barriers for direct elimination of ethyl and 3-methyl groups from $EMMIM^+DCA^-$, which are 2.41 and 2.80 eV, respectively.

B. RRKM Results. To evaluate whether the major initial decomposition paths of $EMIM^+DCA^-$ and $EMMIM^+DCA^-$ identified in trajectory simulations could account for realistic situations, the RRKM program was used to calculate the rates for each of these paths at different temperatures. To calculate the RRKM unimolecular rates, sets of vibrational frequencies and rotational constants appropriate for the reactants and the transition states leading to dissociation are required. These are derived from the frequencies and rotational constants calculated at B3LYP/6-31+G* level, with the frequencies scaled by a factor of 0.955.[27] The rotation quantum number K was treated as active in evaluating the rates $k(E, J)$ so that all $(2J + 1)$ K-levels are counted,[52] i.e.,

$$k(E, J) = \frac{d}{h} \frac{\sum_{K=-J}^{J} G[E - E_0 - E_r^{\dagger}(J, K)]}{\sum_{K=-J}^{J} N[E - E_r(J, K)]} \quad (2)$$

where d is the reaction path degeneracy, G is the sum of states from 0 to $E-E_0-E_r^{\dagger}$ at the transition state, N is the energized reactant's density of states, E is the system energy, E_0 is the unimolecular dissociation threshold, and E_r and $E_r^{\dagger}$ are the rotational energies for the reactant and the transition state, respectively.

Since no reverse activation barrier is located for the proton transfer path of $EMIM^+DCA^-$ and $EMMIM^+DCA^-$, vibrational frequencies appropriate to the proton transfer transition state, hereafter termed TS1 for each ionic liquid, have to be assumed for the RRKM calculations of path **1** decomposition rates for $EMIM^+DCA^-$ and $EMMIM^+DCA^-$, respectively. A set of TS1 vibrational frequencies were chosen for each ionic liquid as follows.[53−57] The vibrational frequencies of TS1 are equal to those of the starting ion pair with removal of only one mode that corresponds to the reaction coordinate (i.e., the stretching mode of the dissociating C−H bond). As long as there is no reverse activation barrier for proton transfer, this choice reflects the "tightest" TS that is possible and would provide lower limits to the unimolecular rates for path **1** of the ionic liquids. A similar approach was used in our recent work on DNB decomposition modeling.[9]

Table 3 summarizes the RRKM results for $EMIM^+DCA^-$ and $EMMIM^+DCA^-$, including their unimolecular rates and decomposition branching ratios at three different temperatures. At each temperature, we have used the averaged internal energy of the system (obtained using the rotational and vibrational partition functions of reactants, see Table 1) for calculations. In Table 3, k_1, k_2, and k_3 represent the rates for crossing TS1, TS2, and TS3 leading from reactants. We have included direct alkyl elimination paths via TS2′ and TS3′ in the RRKM modeling of $EMIM^+DCA^-$ and $EMMIM^+DCA^-$, respectively; however, these paths make little contribution to the decomposition of

dx.doi.org/10.1021/jp5095849 | J. Phys. Chem. A 2014, 118, 11133−11144

the ionic liquids at the simulated temperatures due to the high and tight transition states.

Note that the gas-phase kinetics would be an upper limit to the reaction rates. As concluded in the companion article,[8] using the generic ionic liquid (GIL) model would either keep the barriers the same based on the nucleophilicity analysis of anions, or it would increase the barriers by stabilizing the ion pairs (reactants) relative to the transition states.

As indicated in Table 3, the values of k and branching ratios are temperature-dependent. Even in the case where a tight TS1 is assumed for path **1**, path **1** overwhelmingly dominates the decomposition of $EMIM^+DCA^-$ throughout the whole temperature range of 750−1250 K and dominates the decomposition of $EMMIM^+DCA^-$ at 750 K. Both ionic liquids undergo S_N2 alkyl abstraction reactions. It is interesting to note that $EMIM^+DCA^-$ favors methyl abstraction over ethyl abstraction at all temperatures; while $EMMIM^+DCA^-$, in contrast, favors ethyl abstraction over methyl abstraction except at 750 K where the branching ratio for ethyl abstraction drops to two-thirds of that for methyl abstraction.

It is also noteworthy to realize that the overall decomposition rate of $EMMIM^+DCA^-$ is much lower than that of $EMIM^+DCA^-$ at 750 K, becoming comparable and only slightly higher than $EMIM^+DCA^-$ at 1000 K and exceeding $EMIM^+DCA^-$ by a factor of 3.8 at 1250 K. This scenario can be rationalized as follows. At 750 K, path **1** (i.e., proton transfer) dominates the decomposition of both ionic liquids, and the slow proton transfer rate of $EMMIM^+DCA^-$ is due to the lower acidity of the methyl group at the C2 position. The RRKM predicted that higher stability of $EMMIM^+DCA^-$ compared to $EMIM^+DCA^-$ at this low temperature is consistent with the stability trend detected by TGA of these compounds at similar temperatures.[8] At higher temperatures, ethyl abstraction increases surprisingly quickly for $EMMIM^+DCA^-$ and accounts for more than 60% of its decomposition, resulting in a higher overall decomposition rate of $EMMIM^+DCA^-$ than that of $EMIM^+DCA^-$. The fast increase in ethyl abstraction rate for $EMMIM^+DCA^-$ can be attributed to the properties of the associated transition state TS2. TS2 for $EMMIM^+DCA^-$ has five vibrational frequencies (i.e., 6.2, 14.3, 28.6, 46.1, and 50.7 cm^{-1}) below or equal to 50 cm^{-1} and a total of eight vibrational frequencies below 100 cm^{-1}. However, TS3 for $EMMIM^+DCA^-$ has three vibrational frequencies (i.e., 13.8, 18.6, and 36.9 cm^{-1}) below 50 cm^{-1}, and a total of seven below 100 cm^{-1}. As a result, at 1250 K the sum of states at TS2 is an order of magnitude higher than that at TS3 for $EMMIM^+DCA^-$. Since the rate for crossing each TS is proportional to the sum of states at that TS, the value of k_2 increases dramatically at this temperature. For comparison, in $EMIM^+DCA^-$, TS2 and TS3 have three and four frequencies below 50 cm^{-1}, respectively, and have seven below 50 cm^{-1}. Consequently, $EMIM^+DCA^-$ has a lower number of states at TS2 and thus a lower rate for crossing TS2, compared to either TS3 of the same molecule or TS2 of $EMMIM^+DCA^-$.

In summary, RRKM modeling indicates that path **1** may account for the major decomposition mode in $EMIM^+DCA^-$ and $EMMIM^+DCA^-$, at least at low temperatures. S_N2 methyl and ethyl abstraction would be expected to occur in the decomposition of these two ionic liquids, and their significances increase with increasing decomposition temperature. For $EMMIM^+DCA^-$, ethyl abstraction dominates other decomposition channels at a temperature of 1000 K and above.

V. CONCLUSIONS

Direct dynamics trajectories for thermal decomposition of two ionic liquids, $EMIM^+DCA^-$ and $EMMIM^+DCA^-$, were analyzed to probe their decomposition mechanisms and dynamics. The trajectories, calculated at the B3LYP/6-31G* level of theory, are able to reproduce decomposition products observed in TGA−MS and VUV−PI−TOFMS experiments and reveal various decomposition paths. RRKM theory was used to verify the significance of these decomposition paths and calculate the branching ratios at several decomposition temperatures, based on the reaction coordinates constructed using trajectory results as a guide. According to RRKM analysis, proton transfer and S_N2 abstraction of 1-ethyl and 3-methyl by the DCA^- anion are important processes for both compounds at typical decomposition temperatures. While proton transfer clearly dominates the decomposition of $EMIM^+DCA^-$, its importance (as judged by its branching ratio) decreases in $EMMIM^+DCA^-$ where the hydrogen atom at the C2 position of the imidazolium ring is substituted by a methyl group, and such decrease becomes particularly substantial at a decomposition temperature of 1000 K and above. However, RRKM results imply that the decrease of C2 activity by methyl substitution does not enhance the overall thermal stability of $EMMIM^+DCA^-$ at higher temperatures because of the fast increasing S_N2 ethyl abstraction rate.

AUTHOR INFORMATION

Corresponding Author

*E-mail: jianbo.liu@qc.cuny.edu.

Notes

The authors declare no competing financial interest.

ACKNOWLEDGMENTS

This work was supported by the Air Force Research Laboratory through ERC, Inc. (Subcontract No. RS120241). J.L. also acknowledges support by the National Science Foundation CAREER Award (Grant No. CHE-0954507) and would like to thank Bill Hase (at Texas Tech) for providing the Venus program.

REFERENCES

(1) Arduengo, A. J., III; Harlow, R. L.; Kline, M. A Stable Crystalline Carbene. *J. Am. Chem. Soc.* **1991**, *113*, 361−363.

(2) Hollóczki, O.; Gerhard, D.; Massone, K.; Szarvas, L.; Németh, B.; Veszprémi, T.; Nyulászi, L. Carbenes in Ionic Liquids. *New J. Chem.* **2010**, *34*, 3004−3009.

(3) Handy, S. T.; Okello, M. The 2-Position of Imidazolium Ionic Liquids: Substitution and Exchange. *J. Org. Chem.* **2005**, *70*, 1915−1918.

(4) Chowdhury, A.; Thynell, S. T. Confined Rapid Thermolysis/Ftir/Tof Studies of Imidazolium-Based Ionic Liquids. *Thermochim. Acta* **2006**, *443*, 159−172.

(5) Verevkin, S. P.; Emel'yanenko, V. N.; Zaitsau, D. H.; Heintz, A.; Muzny, C. D.; Frenkel, M. Thermochemistry of Imidazolium-Based Ionic Liquids: Experiment and First-Principles Calculations. *Phys. Chem. Chem. Phys.* **2012**, *12*, 14994−15000.

(6) Chambreau, S. D.; Schneider, S.; Rosander, M.; Hawkins, T.; Gallegos, C. J.; Pastewait, M. F.; Vaghjiani, G. L. Fourier Transform Infrared Studies in Hypergolic Ignition of Ionic Liquids. *J. Phys. Chem. A* **2008**, *112*, 7816−7824.

(7) Schneider, S.; Hawkins, T.; Rosander, M.; Vaghjiani, G.; Chambreau, S.; Drake, G. Ionic Liquids as Hypergolic Fuels. *Energy Fuels* **2008**, *22*, 2871−2872.

(8) Chambreau, S. D.; Schenk, A. C.; Sheppard, A. J.; Yandek, G. R.; Vaghjiani, G. L.; Maciejewski, J.; Koh, C. J.; Golan, A.; Leone, S. R. Thermal Decomposition Mechanisms of Alkylimidazolium Ionic Liquids with Cyano-Functionalized Anions. *J. Phys. Chem. A* **2014**, DOI: 10.1021/jp5095855.
(9) Liu, J.; Chambreau, S. D.; Vaghjiani, G. L. Thermal Decomposition of 1,5-Dinitrobiuret (Dnb): Direct Dynamics Trajectroy Simulations and Statistical Modeling. *J. Phys. Chem. A* **2011**, *115*, 8064−8072.
(10) Liu, J.; Anderson, S. L. Dynamical Control of 'Statistical' Ion−Molecule Reactions. *Int. J. Mass Spectrom.* **2005**, *241*, 173−184.
(11) Wang, I. S. Y.; Karplus, M. Dynamics of Organic Reactions. *J. Am. Chem. Soc.* **1973**, *95*, 8160−8164.
(12) Leforestier, C. Classical Trajectories Using the Full Ab Initio Potential Energy Surface $H^- + CH_4 \rightarrow CH_4 + H^-$. *J. Chem. Phys.* **1978**, *68*, 4406−4410.
(13) Car, R.; Parrinello, M. Unified Approach for Molecular Dynamics and Density Functional Theory. *Phys. Rev. Lett.* **1985**, *55*, 2471−2474.
(14) Baldridge, K. K.; Gordon, M. S.; Steckler, R.; Truhlar, D. G. Ab Initio Reaction Paths and Direct Dynamics Calculations. *J. Phys. Chem.* **1989**, *93*, 5107−5119.
(15) Helgaker, T.; Uggerud, E.; Jensen, H. J. A. Integration of the Classical Equations of Motion on Ab Initio Molecular Potential Energy Surfaces Using Gradients and Hessians: Application to Translational Energy Release Upon Fragmentation. *Chem. Phys. Lett.* **1990**, *173*, 145−150.
(16) Bolton, K.; Hase, W. L. Direct Dynamics Simulations of Reactive Systems. *Modern Methods for Multidimensional Dynamics Computations in Chemistry*; World Scientific: Singapore, 1998; pp 143−189
(17) Hase, W. L., Ed.*Advances in Classical Trajectory Methods, Vol. 1: Intramolecular and Nonlinear Dynamics*; JAI: Greenwich, U.K., 1998.
(18) Sun, L.; Song, K.; Hase, W. L. A Sn2 Reaction That Avoids Its Deep Potential Energy Minimum. *Science* **2002**, *296*, 875−878.
(19) Bakken, V.; Millam, J. M.; Schlegel, H. B. Ab Initio Classical Trajectories on the Born-Oppenheimer Surface: Updating Methods for Hessian-Based Integrators. *J. Chem. Phys.* **1999**, *111*, 8773−8777.
(20) Marcus, R. A. Unimolecular Dissociations and Free-Radical Recombination Reactions. *J. Chem. Phys.* **1952**, *20*, 359−364.
(21) Frisch, M. J.; Trucks, G. W.; Schlegel, H. B.; Scuseria, G. E.; Robb, M. A.; Cheeseman, J. R.; Scalmani, G.; Barone, V.; Mennucci, B.; Petersson, G. A.; et al. *Gaussian 09*, revision B. 01; Gaussian, Inc.: Wallingford, CT, 2009.
(22) Emel'yanenko, V. N.; Verevkin, S. P.; Heintz, A. The Gaseous Enthalpy of Formation of the Ionic Liquid 1-Butyl-3-Methylimidazolium Dicyanamide from Combustion Calorimetry, Vapor Pressure Measurements, and Ab Initio Calculations. *J. Am. Chem. Soc.* **2007**, *129*, 3930−3937.
(23) Verevkin, S. P.; Emel'yanenko, V. N.; Zaitsau, D. H.; Heintz, A.; Muzny, C. D.; Frenkel, M. Thermochemistry of Imidazolium-Based Ionic Liquids: Experiment and First-Principles Calculations. *Phys. Chem. Chem. Phys.* **2010**, *12*, 14994−15000.
(24) Hollóczki, O.; Gerhard, D.; Massone, K.; Szarvas, L.; Németh, B.; Veszprémi, T.; Nyulászi, L. Carbenes in Ionic Liquids. *New J. Chem.* **2010**, *34*, 3004−3009.
(25) Clough, M. T.; Geyer, K.; Hunt, P. A.; Mertes, J.; Welton, T. Thermal Decomposition of Carboxylate Ionic Liquids: Trends and Mechanisms. *Phys. Chem. Chem. Phys.* **2013**, *15*, 20480−20495.
(26) Kroona, M. C.; Buijsc, W.; Petersa, C. J.; Witkamp, G.-J. Quantum Chemical Aided Prediction of the Thermal Decomposition Mechanisms and Temperatures of Ionic Liquids. *Thermochim. Acta* **2007**, *465*, 40−47.
(27) Zheng, J.; Alecu, I. M.; Lynch, B. J.; Zhao, Y.; Truhlar, D. G. Database of Frequency Scale Factors for Electronic Model Chemistries, Version 2, 2010; http://comp.chem.umn.edu/freqscale/version2.htm.
(28) Baer, T.; Hase, W. L. *Unimolecular Reaction Dynamics: Theory and Experiments*; Oxford University Press: New York, 1996.
(29) Hase, W. L. Some Recent Advances and Remaining Questions Regarding Unimolecular Rate Theory. *Acc. Chem. Res.* **1998**, *31*, 659−665.
(30) Fukui, K. A Formulation of the Reaction Coordinate. *J. Phys. Chem.* **1970**, *74*, 461−463.
(31) Zhu, L.; Hase, W. L. *A General Rrkm Program (Qcpe 644), Quantum Chemistry Program Exchange*; University of Indiana: Bloomington, IN, 1993.
(32) Boyle, J. M.; Uselman, B. W.; Liu, J.; Anderson, S. L. Vibrational Effects on the Reaction of NO_2^+ with C_2H_2: Effects of Bending and Bending Angular Momentum. *J. Chem. Phys.* **2008**, *128*, 114304/114301−114304/114312.
(33) Fang, Y.; Liu, J. Reaction of Protonated Tyrosine with Electronically Excited Singlet Molecular Oxygen: An Experimental and Trajectory Study. *J. Phys. Chem. A* **2009**, *113*, 11250−11261.
(34) Hase, W. L.; Bolton, K.; de Sainte Claire, P.; Duchovic, R. J.; Hu, X.; Komornicki, A.; Li, G.; Lim, K.; Lu, D.; Peslherbe, G. H.; et al. *Venus 99: A General Chemical Dynamics Computer Program*; Texas Tech Univeristy: Lubbock, TX, 1999.
(35) Bacskay, G. B. A Quadratically Convergent Hartree-Fock (Qc-Scf) Method. Application to Closed Shell Systems. *Chem. Phys.* **1981**, *61*, 385−404.
(36) Peslherbe, G. H.; Wang, H.; Hase, W. L. Monte Carlo Sampling for Classical Trajectory Simulations. *Adv. Chem. Phys.* **1999**, *105*, 177−201.
(37) Laaksonen, L. *Gopenmol*, 3.0 ed.; Center for Scientific Computing: Espoo, Finland, 2005; https://research.csc.fi/-/gopenmol.
(38) Liu, J.; Song, K.; Hase, W. L.; Anderson, S. L. Direct Dynamics Trajectory Study of the Reaction of Formaldehyde Cation with D_2: Vibrational and Zero-Point Energy Effects on Quasiclassical Trajectories. *J. Phys. Chem. A* **2005**, *109*, 11376−11384.
(39) Liu, J.; Song, K.; Hase, W. L.; Anderson, S. L. Direct Dynamics Trajectory Study of Vibrational Effects: Can Polanyi Rules Be Generalized to a Polyatomic System? *J. Am. Chem. Soc.* **2004**, *126*, 8602−8603.
(40) Liu, J.; Song, K.; Hase, W. L.; Anderson, S. L. Direct Dynamics Study of Energy Transfer and Collision-Induced Dissociation: Effects of Impact Energy, Geometry, and Reactant Vibrational Mode in H_2CO^+-Ne Collisions. *J. Chem. Phys.* **2003**, *119*, 3040−3050.
(41) Liu, J.; Uselman, B.; Boyle, J.; Anderson, S. L. The Effects of Collision Energy, Vibrational Mode and Vibrational Angular Momentum on Energy Transfer and Dissociation in NO_2^+-Rare Gas Collisions: An Experimental and Trajectory Study. *J. Chem. Phys.* **2006**, *125*, 133115.
(42) Liu, J.; Anderson, S. L. The Origins of Large Bending Enhancement of the Reaction of $C_2H_2^+$ with Methane: The Effects of Bending Momentum, Ruling out the Precursor, and Steps Towards Polanyi Rules for Polyatomic Reactions. *Phys. Chem. Chem. Phys.* **2009**, *11*, 8721−8732.
(43) Fang, Y.; Liu, F.; Bennett, A.; Ara, S.; Liu, J. Experimental and Trajectory Study on Reaction of Protonated Methionine with Electronically Excited Singlet Molecular Oxygen ($A^1\delta_g$): Reaction Dynamics and Collision Energy Effects. *J. Phys. Chem. B* **2011**, *115*, 2671−2682.
(44) Untch, A.; Schinke, R.; Cotting, R.; Huber, J. R. The Vibrational Predissociation of *Cis*-Methyl Nitrite in the S_1 State: A Comparison of Exact Quantum Mechanical Wave Package Calculation with Calssical Trajectory Calculations and Detailed Experimental Results. *J. Chem. Phys.* **1993**, *99*, 9553−9566.
(45) Miller, W. H.; Hase, W. L.; Darling, C. L. A Simple Model for Correcting the Zero Point Energy Problem in Classical Trajectory Simulations of Polyatomic Molecules. *J. Chem. Phys.* **1989**, *91*, 2863−2868.
(46) Emel'yanenko, V. N.; Verevkin, S. P.; Heintz, A. The Gaseous Enthalpy of Formation of the Ionic Liquid 1-Butyl-3-Methylimidazolium Dicyanamide from Combustion Calorimetry, Vapor Pressure Measurements, and Ab Initio Calculations. *J. Am. Chem. Soc.* **2007**, *129*, 3930−3937.

(47) Chambreau, S. D.; Boatz, J. A.; Vaghjiani, G. L.; Koh, C.; Kostko, O.; Golan, A.; Leone, S. R. Thermal Decomposition Mechanism of 1-Ethyl-3-Methylimidazolium Bromide Ionic Liquid. *J. Phys. Chem. A* **2012**, *116*, 5867−5876.
(48) Kroon, M. C.; Buijs, W.; Peters, C. J.; Witkamp, G.-J. Quantum Chemical Aided Prediction of the Thermal Decomposition Mechanisms and Temperatures of Ionic Liquids. *Thermochim. Acta* **2007**, *465*, 40−47.
(49) Clough, M. T.; Geyer, K.; Hunt, P. A.; Mertes, J.; Welton, T. Thermal Decomposition of Carboxylate Ionic Liquids: Trends and Mechanisms. *Phys. Chem. Chem. Phys.* **2013**, *15*, 20480−20495.
(50) Dessiaterik, Y.; Nguyen, T.; Baer, T.; Miller, R. E. IR Vaporization Mass Spectrometry of Aerosol Particles with Ionic Solutions: The Problem of Ion-Ion Recombination. *J. Phys. Chem. A* **2003**, *107*, 11245−11252.
(51) Chan, B. K. M.; Chang, N. H.; grimmett, M. R. *Aust. J. Chem.* **1977**, *30*, 2005−2013.
(52) Zhu, L.; Hase, W. L. Comparison of Modes for Calculating the Rrkm Unimolecular Constant K(E,J). *Chem. Phys. Lett.* **1990**, *175*, 117−124.
(53) Meyer, F.; Khan, F. A.; Armentrout, P. B. Thermochemistry of Transition Metal Benzene Complexes: Binding Energies of M-$(C_6H_6)_X^+$ (X = 1, 2) for M = Ti to Cu. *J. Am. Chem. Soc.* **1995**, *117*, 9740−9748.
(54) More, M. B.; Glendening, E. D.; Ray, D.; Feller, D.; Armentrout, P. B. Cation-Ether Complexes in the Gas Phase: Bond Dissociation Energies and Equilibrium Structures of $Li^+[O(CH_3)_2]_X$, X = 1−4. *J. Phys. Chem.* **1996**, *100*, 1605−1614.
(55) Ray, D.; Feller, D.; More, M. B.; Glendening, E. D.; Armentrout, P. B. Cation-Ether Complexes in the Gas Phase: Bond Dissociation Energies and Equilibrium Structures of Li^+(1,2-Dimethoxyethane)$_x$, x = 1 and 2, and Li^+(12-Crown-4). *J. Phys. Chem.* **1996**, *100*, 16116−16125.
(56) Rodgers, M. T.; Armentrout, P. B. Statistical Modeling of Competitive Threshold Collision-Induced Dissociation. *J. Chem. Phys.* **1998**, *109*, 1787−1800.
(57) Rodgers, M. T.; Ervin, K. M.; Armentrout, P. B. Statistical Modeling of Collision-Induced Dissociation Thresholds. *J. Chem. Phys.* **1997**, *106*, 4499−4508.